Environmental Science and Pollution Research
https://doi.org/10.1007/s11356-023-28443-7

Kinetics of carbon dioxide absorption in aqueous blend of 1-(2-aminoethyl) piperazine using a stirred cell reactor

Sukanta Kumar Dash[1] · **Ishanee Sharma**[1]

Received: 20 January 2023 / Accepted: 21 June 2023

Abstract

Carbon capture utilization and storage (CCUS), the technology for decarbonizing carbon dioxide (CO_2) from greenhouse gas emitters such as steel, cement, oil, gas, petrochemicals, chemicals, and fertilizers, has a critical role to play in the world to achieve industrial net zero targets by 2050. CO_2 can be separated from industrial exhaust gases/flue gases using amine-based solvents utilizing the post-combustion CO_2 Capture process. One most crucial solvent characterization for this application is the kinetics of CO_2 absorption. This work identifies aqueous 1-(2-aminoethyl) piperazine (AEPZ) as a potential candidate for CO_2 capture solvent. The kinetics of absorption of CO_2 in aqueous AEPZ is studied using stirred cell reactor. The experiments are performed at temperatures ranging from 303 to 333 K with weight fractions of AEPZ in an aqueous solution ranging from 0.1 to 0.4. One of the critical parameters of the kinetic study is Henry's constant which is determined experimentally using another stirred cell reactor at a similar temperature and pressure range. The experimental data shows that the overall rate constant is $K_{ov} = 2.52987 \times 10^{-4}$ mol/m^{2}s-kPa for 0.1 wt fr. of AEPZ at 313 K with an initial CO_2 partial pressure of 10 kPa. The temperature dependency relation of the second-order reaction rate constant, k_2, is found to be $6.126 \times 10^{11} exp(-5102/T)$ using the Arrhenius equation. The activation energy of 0.3 wt fr. AEPZ is found to be 42.42 kJ/mol. In addition, the density and viscosity of the aqueous solvent are determined at a wide range of temperatures. The diffusivity of CO_2 and physical solubility used in the model development has also been determined. The kinetic parameters obtained from this study are helpful in the process design of CO_2 capture in a regenerative process with a blended solvent with AEPZ.

Keywords CO_2 capture; 1-(2-Aminoethyl) piperazine · Kinetic modeling; Stirred cell reactor · Absorption

Introduction

The rise in anthropogenic CO_2 emissions into the atmosphere has been a significant environmental concern. There has been an increase of 41% in CO_2 concentration in the atmosphere (NOAA 2021), which is a substantial cause of global warming. The most recent decade is the warmest in 6500 years (IPCC 2021), caused by anthropogenic CO_2 emission. The power industry had the highest global CO_2 emissions (44.37%) in 2020, followed by the industries (22.4%) and the transportation sector (20.6%) (Tiseo 2022). Capturing CO_2 from industries and power plants has become critical to reducing anthropogenic CO_2 emissions. Post-combustion capture of CO_2 (PCC) using amine solvent is the most popular technology for CO_2 removal (Aboudheir et al. 2003). However, capturing CO_2 using post-combustion technology is generally difficult due to the low partial pressure of CO_2 in the flue gas stream. As a result, the necessary driving force is limited, and more energy is required to compress CO_2 for capture purposes (Dash and Wadibhasme 2017). The competitive amine solvent should have fast reaction kinetics with CO_2, good absorption capacity, and a low degradation rate (Dey et al. 2018). Traditional amines such as monoethanolamine (MEA), diethanolamine (DEA), diisopropanolamine (DIPA), methyldiethanolamine (MDEA), diglycolamine (DGA), etc., have all been utilized in recent years to absorb acid gases like CO_2 and H_2S from the industries (Kierzkowska-Pawlak et al. 2014). MEA is considered a benchmarked solvent for CO_2 removal, and 30 wt% aqueous MEA has been used in industries for many years (Ying and

Responsible Editor: Tito Roberto Cadaval Jr

✉ Sukanta Kumar Dash
sk.dash@sot.pdpu.ac.in

[1] Department of Chemical Engineering (CO2 Research Group), Pandit Deendayal Energy University, Raisan, Gandhinagar 382426, Gujarat, India

Published online: 15 July 2023

Eimer 2013). Although MEA is highly reactive and low in cost, it has issues such as high regeneration cost, low equilibrium solubility, hazardous degradation products, corrosion to the equipment, and solvent losses. Other solvents used in industry, such as tertiary amines like MDEA, have a reasonable absorption rate and higher absorption capacity than MEA or DEA but have lower kinetics (Kierzkowska-Pawlak et al. 2014). Because of the issues with traditional alkanolamine solvents, researchers are focusing on better alternatives. These alternative solvents should have high reactivity, high equilibrium capacity, favorable physicochemical properties, low oxidative and thermal degradation, high corrosion resistance, low regeneration energy requirement, low environmental impact, and low cost. This combination of properties can not be achieved using a single amine; hence, desirable amines may be combined to develop a suitable one. Nowadays, sterically hindered amines, blended amines, non-amine absorbents, and cyclic amines for the chemical absorption of CO_2 are attractive research areas and gaining momentum.

Cyclic amines have gained lots of interest in the chemical absorption of CO_2. Piperazine (PZ), a cyclic di-amine, is the most popular amine and is widely used as an activator along with sterically hindered amine 2-amine-2methyl-1-propanol (AMP) and MDEA (Dash et al. 2011; Dash et al. 2012; Dash et al. 2014, Dash and Bandyopadhyay 2016). Although PZ and its blend require moderate energy for regeneration, it does not degrade quickly, but it has issues like precipitation and is less soluble in water at low temperatures. Dey et al. (2018) studied CO_2 solubility in a blended solvent of MDEA and AEPZ. The author reported that the blended solvent showed better CO_2 loading capacity than MDEA. Hence, AEPZ can be easily used as a rate promoter in MDEA or other solvents. Dey et al. (2019) reported the solubility of CO_2 in AEPZ + H_2O, including the density and viscosity of aqueous AEPZ solutions at different concentrations and temperatures. Fang et al. (2020) analyzed the viscosities and diffusivities of 0.1 to 1. mass fraction aqueous solutions of AEPZ at temperatures ranging from 303 to 323 K. Although some literature on AEPZ is available in the solubility, density, and viscosity studies, the literature on the kinetic analysis of CO_2 in aqueous AEPZ for CO_2 capture application is minimal.

Paul et al. (2009a) studied the kinetics of the solvent blends of AEPZ + MDEA using a wetted wall column experimental setup. They found that the CO_2 reaction rate with AEPZ increased, with its concentration in the mixture confirming its role as an activator in a mixed solvent. Paul et al. (2009b) conducted the kinetic study of AEPZ using a wetted-wall column and considered AEPZ concentrations ranging from 0.083 to 1.266 kmol/m^3. Their study revealed that the second-order reaction rate constant was higher than that of PZ. Investigating the kinetics in alternative experiments is essential to confirm the findings and to better design the absorber and desorber units in a PCC process. As CO_2 absorption in amine solution is a mix of mass transfer and chemical reaction, it is tough to get precise kinetics data (Lu et al. 2019). The stability of temperature, pressure, and the gas–liquid contact area is essential for obtaining accurate kinetics data.

The kinetic study can be conducted in different types of reactors. So far, the kinetics study of CO_2 absorption in AEPZ has been performed in a wetted wall column (Paul et al. 2009b) but not verified using other reactors. The stirred cell reactor is one such reactor to examine the kinetics as it is simple to build and operate and requires less supporting equipment (Ying and Eimer 2013). The reactor used in our study is a cylindrical reactor with a stirrer, and baffles are present in the reactor to avoid the formation of the vortex. The main advantage of stirred cell reactor is that only the pressure drop of the gas is required to measure, but many modeling equations are needed to determine the rate constant. CO_2 absorption in amine solvent is usually based on surface renewal theory when stirred cell reactor is used, but in some cases, CO_2 absorption experiments were carried out using film theory. Film theory applies when the establishment time for the concentration gradient is very short in relation to the transfer time. The reaction is confined in a very thin film because the CO_2 absorption reaction in amine solvent is very fast, and the establishment time for the gradient to develop is very short (Coulson et al. 1999). In this case, the film and surface renewal theories produce similar results (Danckwerts et al. 1963).

Kinetics studies usually lead to mechanistic conclusions about the mechanism of CO_2 capture by amines. Exhaustive discussion on mechanistic findings about the mechanism of CO_2 capture by amines can be found in the literature (Vaidya and Kenig 2007; Aboudheir et al. 2003; Ying and Eimer 2013; Lu et al. 2019; Kierzkowska-Pawlak et al. 2014. From the literature, it is found that the conclusions of the amine-CO_2 reaction mechanism are almost the same as reported by many authors. Hence, an exhaustive discussion has not been included in this article (Vaidya and Kenig 2007).

In view of the above discussions, this work focuses on the kinetic study of CO_2 absorption in an aqueous AEPZ solution using a stirred cell reactor. The important physicochemical properties such as density, viscosity, diffusivity, and Henry's constant have been determined in this work. The diffusivity is calculated from the viscosity and N_2O analogy following the method described by Li et al. (2014). These properties are required for analyzing absorption kinetics studies. The kinetic studies and Henry's constant determination have been carried out at the AEPZ concentrations of 0.1 w to 0.4 w at 313 K. The temperature considered for the experiments is 303 to 333 K for 0.3 w AEPZ. The kinetic parameters and the absorption rate of CO_2 in AEPZ have been calculated from the experimental data. The Arrhenius

equation from the second-order reaction rate coefficient has also been developed and reported. These data will help establish kinetic rate equations for the blended solvents ongoing with our research group. Understanding of reaction meachnism is necessary for obtaining the Arrhenius constant (k_2), and k-oversed (k_{obs}), for CO_2 reaction with aqueous AEPZ. The reaction mechanism of AEPZ is complex because of the presence of three amine groups by which many intermediates are formed. Few authors reported the reactions when CO_2 reacts with aqueous AEPZ to the possible formation of mono-, di-, and tri-amine carbamates but considered only mono-carbamate (Dey et al. 2019; Paul et al. 2009b; Choi et al. 2016). The tertiary amine has a too-small protonation constant that its effect on the chemical reaction can easily be neglected if the Brønsted relation is considered (Paul et al. 2009b). Considering both the primary and the secondary amines form carbamates, the kinetic and equilibrium reactions in which CO_2 reacts with aqueous AEPZ are given by reactions R1 to R7.

Physical solubility: The CO_2 molecule in the gas phase is to diffuse in the liquid phase following Henry's law of gas solubility as per reaction (R1)

$$CO_2(g) \overset{H_{CO_2}}{\rightarrow} CO_2(aq) \tag{R1}$$

Water disassociation, CO_2 hydration, and bicarbonate ion disassociation: In the aqueous liquid phase, water dissociation occurs according reaction (R2). Once the CO_2 dissolves in the aqueous liquid phase, it then reacts with water to form carbonates and bicarbonates as per the reactions (R3) and R4

$$H_2O \leftrightarrow H^+ + OH^- \tag{R2}$$

$$HCO_3^- + H_2O \leftrightarrow H_3O^+ + CO_3^{2-} \tag{R3}$$

$$CO_2 + H_2O \leftrightarrow HCO_3^- + H^+ \tag{R4}$$

AEPZ protonation carbamate hydrolysis: In the aqueous medium with the presence of CO_2, AEPZ undergoes protonation and AEPZ carbamate formation, shown in reactions R6 and R7, respectively.

$$AEPZH^+ \leftrightarrow AEPZ + H^+ \tag{R5}$$

$$AEPZCOO^- + H_2O \leftrightarrow AEPZ + HCO_3^- \tag{R6}$$

The contribution of equilibrium reaction to the overall rate is negligible, as described by Paul et al. (2009b). and ignored in the prevailing rate. The main specie that participates in the overall kinetics is the AEPZ carbamates. The carbamates are formed for both primary and secondary amines as both the amine groups can react to form carbamates. It is tough to find out the contribution of each group to the overall carbamate formation. The overall reaction rate of aqueous AEPZ with CO_2 can be represented by reaction R7 clubbing all the isomers of AEPZ carbamates into a single carbamate, as proposed by Paul et al. 2009b.

$$CO_2 + AEPZ + b \rightleftharpoons AEPZCOO - + bH^+ \tag{R7}$$

where b is any base and $AEPZCOO^-$ is the carbamate of AEPZ. For the kinetic analysis, it is assumed that the CO_2-AEPZ reaction has pseudo-first-order kinetics, i.e., first-order with respect to AEPZ and CO_2. This assumption's underlying conditions and validity are explained later in the "Results and discussion" section, estimation of k_2. Hence, the rate of reaction of CO_2 with AEPZ is given by Eq. 1 (Paul et al. 2009b).

$$r_{CO_2-AEP} = k_2\left[CO_2\right][AEPZ] = k_{obs}\left[CO_2\right] \tag{1}$$

where k_2 is the rate constant of the second-order reaction, and k_{obs} are the pseudo-first-order reaction rate constant. The value of k_2 and k_{obs} has been obtained by systematic experiment and data interpretation which is explained in the material and method section.

Materials and methods

AEPZ (99%) is purchased from Sigma-Aldrich (USA), and CO_2 (99% purity) and N_2O cylinders are procured from Linde (India). 0.1 w, 0.2 w, 0.3 w, and 0.4 w aqueous AEPZ solutions are prepared using AEPZ (99%) and distilled water (Millipore, USA). The solvents are prepared by weight and measured on a precision measuring scale (ME204, Mettler Toledo) of accuracy ± 0.001.

Measurement of density and moldeling

The densities of various AEPZ solvents are measured using an oscillating-tube density meter (Anton Parr, DMA 4500). This density meter has a Peltier temperature controller to measure the density at different temperatures. The instrument is calibrated with air and distilled water following standard procedure. Methanol is injected into the density meter to clean the oscillation tube, and then the air bubbles are removed with the help of the built-in air bubble removal system. The density measurement temperature range and solvent name are set. The solvent is then injected into the density meter's oscillating tube, and its density is measured throughout a defined temperature range.

The density of various concentrations of aqueous AEPZ is modeled using the Redlich–Kister equation. The Redlich–Kister equation is written in terms of excess volume (V^E). The

excess volume can be related to the related to density, as given by Eq. (2) (Li et al. 2014).

$$V^E = \frac{x_A M_A + x_w M_w}{\rho_m}\left(x_A \frac{M_A}{\rho_A} + x_w \frac{M_w}{\rho_w}\right) \tag{2}$$

Here, M_A and M_w are the molecular weights of AEPZ and water, respectively. ρ_m is the density of the mixture; ρ_A and ρ_w are the densities of pure AEPZ and water, respectively.

The Redlich–Kister equation is given by Eq. 3. (Dey et al. 2019)

$$V^E = x_A x_w \sum_{i=0}^{N} A_i \left(x_A - x_w\right)^i \tag{3}$$

where x_A is the mole fraction of AEPZ and x_w is the mole fraction of water. A_i is the pair parameter. It is given by Eq. 4.

$$A_i = a + b(T) + c(T)^2 \tag{4}$$

Measurement of viscosity

The kinematic viscosity is measured using a Canon-Fenske viscometer immersed in a constant temperature viscosity bath. Supplied by Alliance Technologies (India) with standards of ASTM D 455. The kinematic viscosity bath consists of an illumination facility for better visibility, a stirrer for better uniformity of temperature throughout the chamber, and a temperature controller with an accuracy of ± 0.1 K. The viscometer tube is rinsed properly with acetone, dried before each experiment, and placed in the thermostated viscosity bath. The temperature of this bath is controlled using a Multispan temperature controller (UTC 421P). The viscometer is used to determine the viscosity of water to standardize it. The viscometer is filled with 8–10 mL of water and then immersed in the viscosity bath. The temperature of the bath is set to the desired level. When the bath reaches the desired temperature, suction is applied to the viscometer until the water reaches the upper marking of the lower bulb. The water would then flow from the lower bulb's upper making to the lower bulb's lower marking. A stopwatch with an accuracy of 0.1 s is used to record the time of flow (t_w). The experiment is repeated at the desired temperature range of 298–348 K. The viscosity of water is calculated using Eq. 5

$$\vartheta = viscometer\ constant \times t_w \tag{5}$$

where ϑ is the solvent's kinematic viscosity in centistokes (cSt) and t_w is the flow time for the reference water.

Dynamic viscosity (μ) is calculated using Eq. 6.

$$\mu_w = \vartheta \times \rho_w \tag{6}$$

where μ_w is the dynamic viscosity of water in centipoise (cP) and ρ_w is the Density of water.

The Viscosity of the solution is obtained using the correlation given in Eq. 7.

$$\mu_s = \frac{\rho_s \times t_s \times \mu_w}{\rho_w \times t_w} \tag{7}$$

where μ_s is the dynamic viscosity of the solution in centipoise (cP), ρ_s is the density of the solution, and t_s is the flow time of the solution. The experimental viscosity values are correlated using a modified Redlich–Kister equation regarding deviation in kinematic viscosity using Eq. 8 as described by Dey et al. (2019).

$$\delta\vartheta = x_A x_w \sum_{i=0}^{N} A_i \left(x_A - x_w\right)^i \tag{8}$$

In Eq. 8, ϑ represents the kinematic viscosity and A_i is a pair parameter. Equation 9 expresses a correlation of the pair parameter in terms of temperature. The deviation in kinematic viscosity is represented by Eq. 10.

$$A_i = a + \frac{b}{T + c} \tag{9}$$

$$\delta\vartheta = \vartheta_m - \left(\vartheta_A x_A + \vartheta_w x_w\right) \tag{10}$$

where ϑ_m is the kinematic viscosity of the mixture, ϑ_1 and ϑ_2 are the kinematic viscosities of pure AEPZ and water, respectively.

Henry's constant measurement

For the measurement of Henry's constant of CO_2 in the solvent, the N_2O analogy method has been adapted as described by Versteeg and van Swaaij (1988). As CO_2 reacts with the solvent, Henry's constant of CO_2 in amine cannot be determined directly. These parameters are determined by using the N_2O analogy, as N_2O does not react with the amine solvent. The apparatus used to measure Henry's constant is similar to that used for kinetics measurement in this work as described in Fig. 1. The only difference is N_2O gas is used instead of CO_2, which is used in kinetic experiments. The reactor is well connected to the buffer vessel, which stores N_2O, and well equipped with valves to regulate N_2O flow. Before the solubility measurement, the system was placed in the water bath, and the temperature was controlled by the temperature controller (make: Julabo). A vacuum was first applied to the buffer vessel to remove any dissolved gases or air in it. Then, N_2O was filled into the tank. The vacuum was also applied in the reactor vessel to

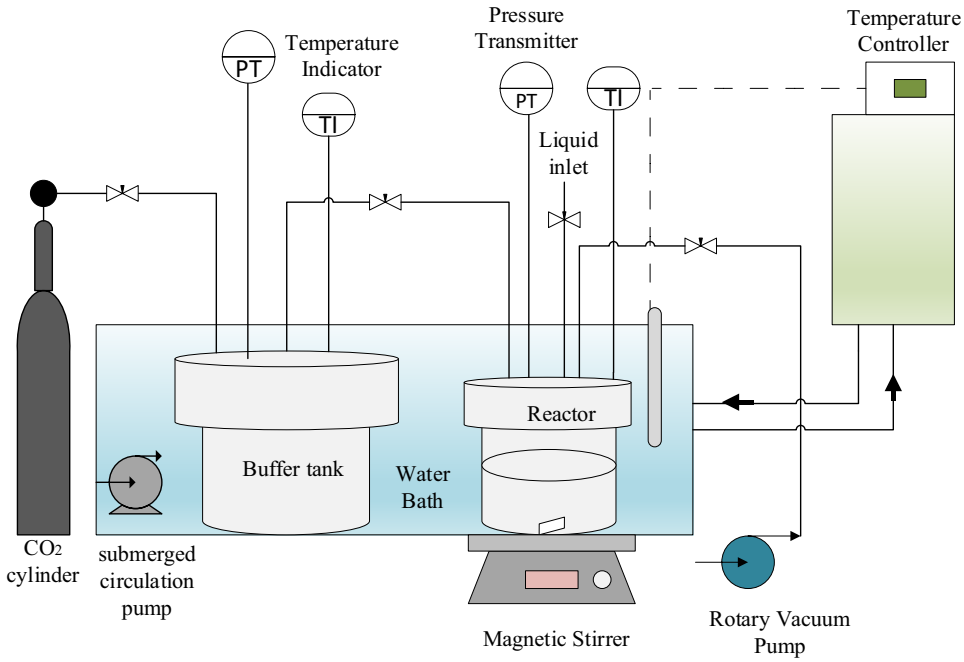

Fig. 1 Schematic diagram of stirred cell experimental setup

remove air and other gases. Two hundred milliliters of aqueous AEPZ solvent was introduced into the reactor, and the dissolved gases were removed by applying a short vacuum. The vapor pressure of the solvent was noted at a constant temperature which was the initial pressure in the reactor. The connecting valve was opened, and N_2O was allowed to flow to the reactor till the experimental pressure was achieved. The system was left for 3–4 h for equilibrium, and the equilibrium pressure was noted. This experiment was repeated for different pressures, to obtain Henry's constant.

The partial pressure of N_2O is the difference between the initial total pressure and the solvent vapor pressure, and by applying Dalton's law, we get Eq. 11

$$P_{N_2O} = P_{total} - P_{start} \tag{11}$$

Henry's constant is calculated using Henry's law and is given in Eq. 12.

$$H_{N_2O} = \frac{P_{N_2O}}{C_{N_2O}} \tag{12}$$

Here, P_{N_2O} is the partial pressure of N_2O in the gas phase, and C_{N_2O} is the concentration of N_2O in the liquid phase. In this work, C_{N2O} is calculated by the mass balance of N_2O in the liquid and gas phases by following the standard method proposed by Park and Sandall (2001). Henry's constant of N_2O and CO_2 in water is determined by using Eqs. 13 and 14, respectively, as proposed by Ying and Eimer (2013).

$$H_{N_2O-H_2O} = 8.55 \times 10^6 \times exp\left(\frac{-2284}{T}\right) \tag{13}$$

$$H_{CO_2-H_2O} = 2.82 \times 10^6 \times exp\left(\frac{-2044}{T}\right) \tag{14}$$

Henry's constant of CO_2 in AEPZ can be calculated using the N_2O analogy (Versteeg and van Swaaij (1988)). It is given by Eq. 15.

$$H_{CO_2-AEP} = H_{N_2O-AEP} \times \left(\frac{H_{CO_2-H_2O}}{H_{N_2O-H_2O}}\right) \tag{15}$$

Determination of diffusivity

The diffusivity of CO_2 in AEPZ cannot be directly determined as CO_2 reacts with AEPZ. It can be determined from the modified Stokes–Einstein correlation in terms of the viscosity of AEPZ and water and the diffusivity of CO_2 in water. The diffusivity of CO_2 in H_2O can be estimated using Eq. 16 as proposed by Versteeg and van Swaaij (1988).

$$D_{CO_2-H_2O} = 2.35 \times 10^{-6} \times exp\left(\frac{-2119}{T}\right) \tag{16}$$

The diffusivities of CO_2 in aqueous AEPZ are calculated using a modified Stokes–Einstein correlation. It is given by Eq. 17.

$$D_{CO_2-AEP} \times \mu_{AEP}^{0.8} = D_{CO_2-H_2O} \times \mu_{H_2O}^{0.8} \tag{17}$$

Kinetics measurements

Apparatus and experimental procedure

The experiments for the kinetics of CO_2 absorption in AEPZ solvent are done in stirred cell batch reactors. The experimental setup and the connectivity to various components of the structure are shown in Fig. 1. The reactor and the buffer vessel are made of stainless steel. They are immersed in a water bath to ensure uniform temperature distribution. The water bath is connected to the circulation temperature controller (Pt 100, Julabo, FRG.) with an accuracy of ± 0.1 K, which controls the temperature of the water bath. The reactor has gas and liquid inlet tubes with needle valves (Swagelok) to regulate the flow of the gas and the liquid. A pressure transmitter (0–100 psia, Rosemount 2051 T, Emerson Process Management, USA) of accuracy ± 0.065% is mounted on the reactor. It measures the CO_2 pressure in the reactor during the absorption reaction. The reactor is connected to a buffer vessel (volume 1254 ml) which stores CO_2 gas. CO_2 is transferred from the buffer vessel to the reactor whenever required during the experiments. The connecting tube has a needle valve (Swagelok) to regulate and stop the flow of CO_2 from the buffer cell to the reactor cell. The whole reactor system is kept on the magnetic stirrer (5 mlh, Remi Instruments Ltd., India), which stirs at 180–190 rpm. The vacuum pump (Oiled Rotary Vacuum Pump, Parag Engineering, India) provides the vacuum to remove dissolved gases in the reactor.

At the start of the experiment, the circulator temperature controller was set at the desired reaction temperature. The buffer vessel and the reactor cell were allowed to reach the equilibrium temperature. A vacuum was applied to both cells to remove the air inside the cells. The buffer vessel was filled with pure CO_2 with a pressure of up to 6000 kPa. A 50 ml amine solution sample was injected into the cell through the inlet. Dissolved gases in the liquid were removed by applying a short vacuum to the reactor cell. The pressure inside the cell was then measured by the pressure transducer, the solvent vapor pressure, p_v. The initial buffer pressure was noted with a pressure transmitter attached to it. The valves connecting the buffer vessel and the reactor were opened to transfer CO_2 from the buffer vessel to the reactor. The valves were closed after the reactor was filled with CO_2, which is the total pressure P_{total}. The total pressure started decreasing as soon as CO_2 was getting absorbed in the solution. The decrease in pressure was noted down for 2–3 min.

The CO_2 partial pressure (P_{CO_2}) is obtained from the difference between the total pressure and the solvent vapor pressure assuming the applicability of Dalton's law.

$$P_{CO_2} = P_{total} - P_V \tag{18}$$

The moles of CO_2 in the gas phase are calculated by Eq. 19, assuming that the ideal gas law is applicable.

$$n_{CO_2} = \frac{PV}{RT} \tag{19}$$

where R is the gas constant, V is the molar volume of the gas, and T is the temperature of the gas.

The absorption flux is calculated by using Eq. 20 during the time interval t in seconds.

$$Flux = \frac{n_1 - n_2}{Interfacial\ Area \times t} \tag{20}$$

Here, n_1 and n_2 are the initial and final moles of CO_2, respectively, in the reactor between the time interval t.

Estimation of kinetics

The kinetics experiments on CO_2 absorption are conducted in the stirred cell reactor. The kinetics measurement of 10 wt% AEPZ, 20 wt% AEPZ, 30 wt% AEPZ, and 40wt% AEPZ at 40 °C and kinetics measurements of 30 wt% AEPZ at 30 °C, 50 °C, and 60 °C were conducted in stirred cell reactor 1. The dimensions of the stirred cell reactor are shown in Table 1. The stirrer is kept at 180 rpm for enough surface renewal to take place.

Absorption flux of the CO_2 (J_{CO_2}) in the aqueous AEPZ solvent is given by (flux = coefficient × driving force) and presented in Eq. 21.

$$J_{CO_2} = K_{ov} p_{CO_2} \tag{21}$$

where K_{ov} is the overall mass transfer coefficient in mol/m^2-s-kPa and p_{CO_2} is the partial pressure of CO_2 in kPa. Flux is plotted against the partial pressure of CO_2. K_{ov} is the slope obtained from the plot. The flux calculation is presented in Table S7. The plot between the partial pressure of CO_2 and flux is presented in Fig. S1.

Estimation of k_L

The liquid phase mass transfer coefficient (k_L) is determined experimentally. k_L depends on the immersion of the stirrer into the liquid in stirred cell reactor. It can be estimated by using Eq. 22 as suggested by Bhosale & Mahajani (2013).

$$\ln\left[\frac{P_t - P_{final}}{P_{initial} - P_{final}}\right] = -\frac{mV_L + V_G}{V_L V_G} k_L A t \tag{22}$$

where P_t is the pressure at a particular time, $P_{initial}$ is the initial pressure, P_{final} is the pressure at the end of the experiment, m is the dimensionless solubility, V_L is the volume of the liquid, V_G is the volume of gas, A is the interfacial area,

and t is the contact time. The dimensionless solubility is represented by Eq. 23.

$$m = \left(\frac{P_{initial} - P_{final}}{P_{final} - P_{vap}}\right)\frac{V_G}{V_L} \tag{23}$$

The stirred cell reactor dimensions are presented in Table 8. To find the value of k_L, $ln\left[\frac{P_t - P_{final}}{P_{initial} - P_{final}}\right]$ is plotted against t. The plot is given in Fig. S2. The obtained value of k_L is 1.36×10^5 m/s.; calculated from the slope of the graphs and the correlations described.

Estimation of k_2

The observed kinetic constant of CO_2 in aq. AEPZ can be given as (Monteiro et al. 2015).

$$k_{obs} = \frac{H^2_{CO_2,AEP}}{D_{CO_2}}\left(\frac{1}{K_{ov}} - \frac{1}{k_G}\right)^{-2} \tag{24}$$

where k_G represents the gas-phase mass transfer coefficient. In this experiment, k_G has been neglected because the experiment has been conducted under vacuum conditions, and pure CO_2 has been used. The gas-phase resistance under this condition is negligible. Incorporating this assumption in Eq. 24, we get Eq. 25 for the obsorbed kinetics.

$$k_{obs} = H^2_{CO_2,AEP}\frac{K^2_{ov}}{D_{CO_2}} \tag{25}$$

The overall rate of reaction of CO_2 in aq. AEPZ is given by

$$-r_{CO_2} = k_{obs}\left[CO_2\right] \tag{26}$$

where $-r_{CO_2}$ is reaction rate of CO_2, m^3/mol-s and $\left[CO_2\right]$ is the concentration of CO_2 in the liquid phase.

The reaction between CO_2 and amine is normally of second order and can be presented by Eq. 27.

$$-r_{CO_2} = k_2\left[CO_2\right][AEPZ] \tag{27}$$

Here, k_2 is the second-order reaction rate constant, L/mol-s and $[AEP]$ is the AEPZ concentration, mol/L.

Rearrangeing the Eqs. 25 and 26, we get Eq. 28.

$$k_{obs} = k_2[AEPZ] \tag{28}$$

For the fast pseudo-first-order reaction regime, the conditions of absorption of CO_2 in AEPZ are given by Eq. 19 (Ying and Eimer 2013):

$$3 < Ha^{\varepsilon}E_i \tag{29}$$

Ha represents the Hatta number, and E_i represents the instantaneous enhancement factor. Pseudo-first order assumption for the fast reaction is feasible only if the kinetic experiments are conducted at very low pressure. The Hatta number of the gas–liquid reaction is calculated using Eq. 30, as suggested by Ying and Eimer (2013).

$$Ha = \frac{\sqrt{\left(\frac{2}{m+1}\right)k_{m,n}C_A^{m-1}C_l^n D_A}}{k_L} \tag{30}$$

Here, $k_{m,n}$ is reaction constant of $(m,n)^{th}$ order, C_A is the concentration of gas, C_l is the concentration of liquid, and k_L is the mass transfer coefficient in the liquid phase. Ha, for the reaction of CO_2 with AEPZ is

$$Ha = \frac{\sqrt{k_2[AEPZ]D_{CO_2}}}{k_L} \tag{31}$$

The instantaneous enhancement factor for CO_2 reaction with aq. AEPZ is given by

$$E_i = 1 + \frac{[AEPZ]}{z \times [CO_2]}\frac{D_{AEP}}{D_{CO_2}} \tag{32}$$

where z is the stoichiometric coefficient of AEPZ solvent. Equation 32 is only applicable to film theory. If the condition given in Eq. 29 is met, then we have

$$E = Ha \tag{33}$$

E represents the enhancement factor. The specific rate of absorption of CO_2 in AEPZ is calculated using Eq. 33, as suggested by Paul et al. (2009a, b).

$$N_{CO_2} = \frac{H_{CO_2}}{p_{CO_2}}\sqrt{k_2[AEPZ]D_{CO_2}} \tag{34}$$

Results and discussion

Density determination

The experimental data for the measurement of density is given in Table 2. The experimental error calculated using error propagation theory (Dey et al. 2018) is reported in the result table. The experimental density data are compared to the literature data (Dey et al. 2019). The comparison is presented in Fig. 2. It is found from Fig. 2 that there is a marginal difference between the results. The linear regression was carried out to fit the experimental data into Eqs. 3 and 4 using Origin software (Verson-2021). The obtained parameters and the formula for calculating % AAD are given in the supplementary material in Table S1. The

Table 1 Stirred cell reactor dimensions

Parameter	Symbol	Value	Unit
Volume of reactor	V	0.521×10^{-3}	m^3
Liquid phase volume	V_L	0.05×10^{-3}	m^3
Stirrer revolutions	rps	3	rps

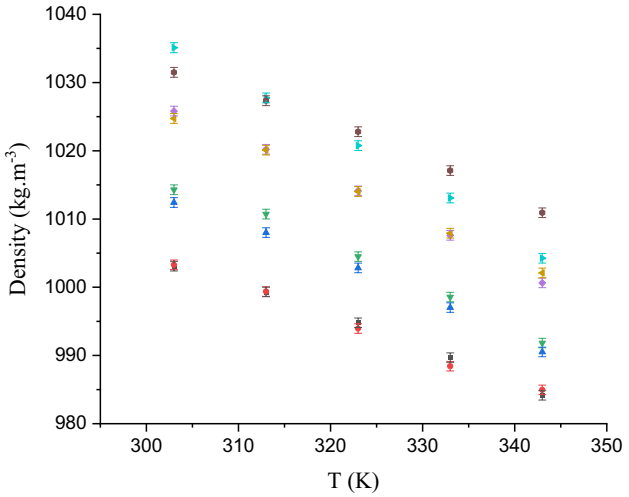

Fig. 2 Density of aqueous AEPZ at various temperature and composition (mass fraction): ●, (0.1 w AEPZ Dey et al., 2019); ▲, (0.2 w AEPZ, this work); ▼, (0.2 w AEPZ, Dey et al., 2019); ◆, (0.3 w AEPZ, this work); ◀, (0.3 w AEPZ, Dey et al., 2019); ▶, (0.4 w AEPZ, this work); ⬢, (0.4 w AEPZ, Dey et al., 2019)

densities predicted by the model do not vary much from the experimental densities, which means that they are in good agreement with each other. The comparison between the model-predicted and experimental data is presented in Fig. 3. The data for the model-predicted densities are given in Table S2. The % AAD for the density of aqueous AEPZ solutions is found to be 0.0796. This result shows that the densities calculated using the equations and the experimental densities are in good agreement with each other. The Redlich–Kister equation can accurately predict the density of the binary solutions. The excess molar volumes of aqueous AEPZ solutions are shown in Fig. 4. From Fig. 4, it can be observed that the excess volumes of AEPZ + H_2O are negative. The excess volumes become more negative as concentration increases. It can be because of the strengthening of dipole–dipole interactions with an increase in the concentration of AEPZ in H_2O. The hydrogen bonding increased as the concentration of AEPZ in water increased. Because of the strong dipole–dipole interaction, volume contraction occurs, resulting in negative values for excess volumes. The negative values of V^E indicate a good structural packing effect, as Das et al. (2017) described. The data

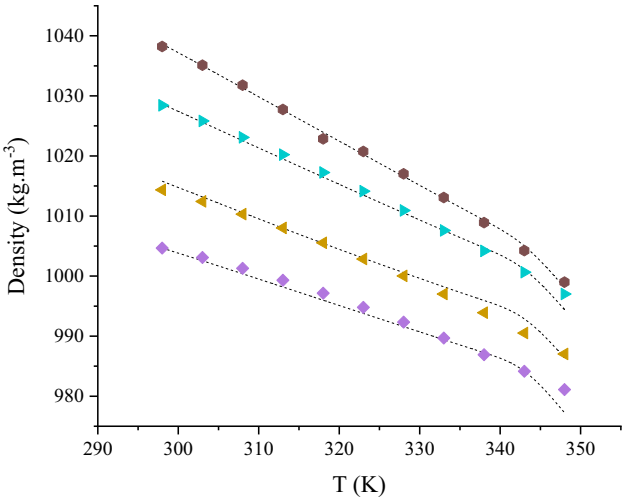

Fig. 3 Comparison of model predicted density of aqueous AEPZ with experimental results at various temperature and composition (mass fraction): ◆, 0.1w AEPZ; ◀, 0.2w AEPZ; ▶, 0.3w AEPZ; ⬢, 0.4w AEPZ; dashed lines -- model predicted Density

for excess volume properties of aqueous AEPZ is presented

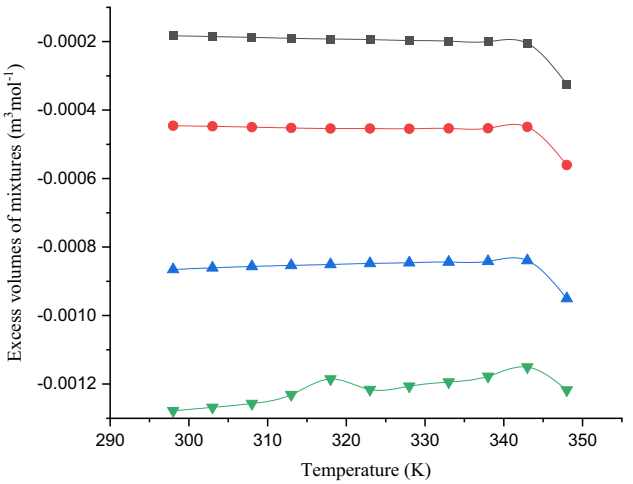

Fig. 4 Model predicted Excess Volume of Mixtures (AEPZ + H2O): ■, (0.1w AEPZ); ●, (0.2w AEPZ); ▲, (0.3w AEPZ); ▼, (0.4w AEPZ)

in Table S3 of the supplementary material.

Viscosity determination

The viscosities of the aqueous AEPZ solutions were measured using a Cannon–Fenske viscometer. The experimental data for the viscosity measurement is presented in Table 3. The observed values are compared to those given by Fang et al. (2020) in Fig. 5.

Table 2 Densities of aqueous AEPZ

Density, kg m^{-3}				
T/K	wt fraction AEPZ			
	0.1 w	0.2 w	0.3 w	0.4 w
298	1004.66	1014.35	1028.41	1038.23
303	1003.09	1012.42	1025.82	1035.11
308	1001.29	1010.30	1023.08	1031.78
313	999.31	1008.01	1020.22	1027.74
318	997.15	1005.54	1017.24	1022.84
323	994.8	1002.83	1014.13	1020.75
328	992.33	1000.02	1010.92	1017.01
333	989.69	997.01	1007.60	1013.08
338	986.91	993.90	1004.18	1008.90
343	984.15	990.51	1000.63	1004.24
348	981.10	987.02	997.02	998.99

The standard uncertainties (u) associated with the measured quantity are $u(T) = 0.1$ K, $u(y) = 0.001$, $u(\rho) = 0.796$ kg m^{-3}, solvent = water

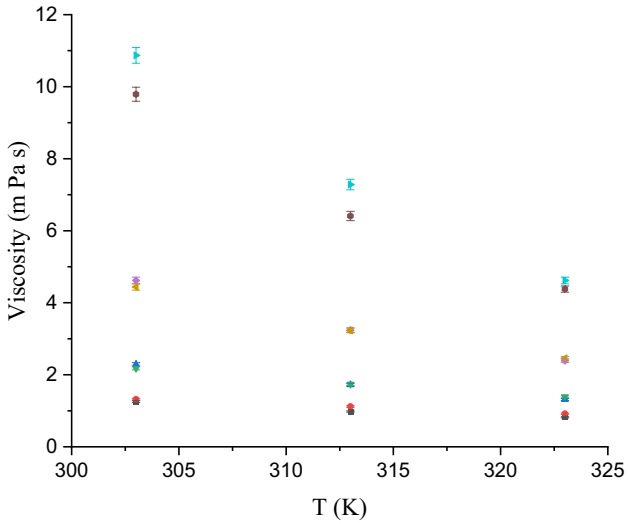

Fig. 5 Viscosity of aqueous AEPZ at various temperature and composition (mass fraction): ■, (0.1w AEPZ, this work); ●, (0.1w AEPZ, Fang et al., 2020); ▲, (0.2w AEPZ, this work); ▼, (0.2w AEPZ, Fang et al., 2020); ◆, (0.3w AEPZ, this work); ◀, (0.3w AEPZ, Fang et al., 2020); ▶, (0.4w AEPZ, this work); ⬢, (0.4w AEPZ, Fang et al., 2020)

The parameters are determined by conducting linear regression of the experimental data using Origin software (Verson-2021) and presented in Table S4 in the supplementary material. Figure 6 shows the comparison between the model-predicted data and the experimental data. From Fig. 6, it can be observed that the Redlich–Kister equation is reasonably accurate for predicting the solvent's viscosity. The obtained % AAD between the predicted and the experimental data is 2.02. The model-predicted viscosity

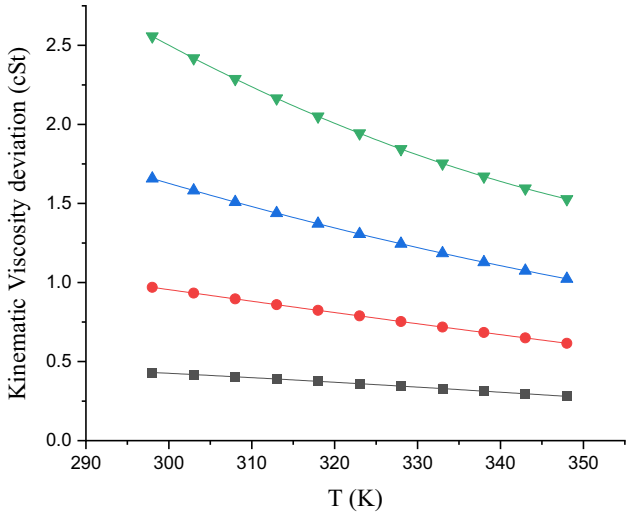

Fig. 6 Kinematic viscosity deviation of aqueous AEPZ at various temperature and composition (mass fraction): ■, (0.1w AEPZ); ●, (0.2w AEPZ); ▲, (0.3w AEPZ); ▼, (0.4w AEPZ)

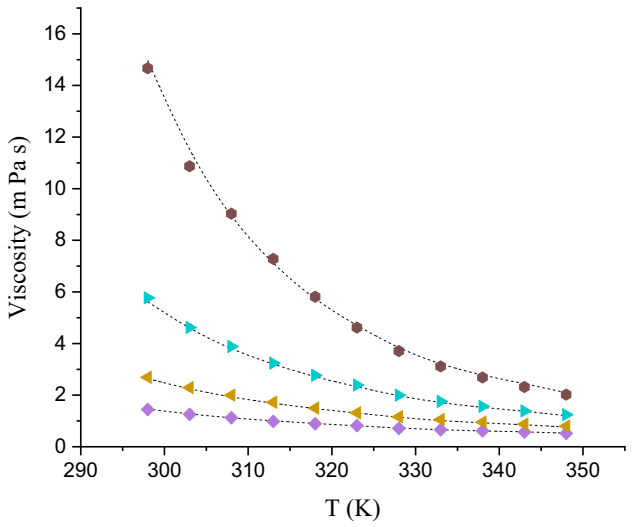

Fig. 7 Comparison of model predicted density of aqueous AEPZ with experimental results at various temperature and composition (mass fraction): ◆, (0.1w AEPZ); ◀, (0.2w AEPZ); ▶, (0.3w AEPZ); ⬢, (0.4w AEPZ); Dashed lines -- model predicted Viscosity

data is given in Table S5. The viscosity deviation data is presented in Fig. 7. The viscosity deviation is positive for all the concentrations of AEPZ. It means that the interactions between AEPZ and water are strong at all concentrations (Vogel and Weiss 1982). The deviations increased with increasing concentrations which indicated that the dipole interactions became stronger with increasing concentrations. The deviations decreased with increasing temperatures indicating that the dipole interactions weakened with increasing temperatures. The data for viscosity deviation is given in Table S6.

From the viscosity data, it is possible to estimate the enthalpy (ΔH), entropy (ΔS), and Gibbs free energy (ΔG) of AEPZ + H_2O using the thermodynamic relation, as suggested by (Águila-Hernández et al. 2008; Das et al. 2017. This relation is represented in Eq. 35.

$$\mu = \left(\frac{hN_A}{V_M}\right) exp\left(\frac{-\Delta S}{R}\right) exp\left(\frac{\Delta H}{RT}\right) \tag{35}$$

Here, h is Planck's constant, N_A is Avogadro's number, V_M is molar volume, and R is the gas constant. Equation 35 can be rearranged to obtain Eq. 36 (Das et al. 2017)

$$Rln\left(\frac{\mu V_M}{hN_A}\right) = \frac{\Delta H}{T} - \Delta S \tag{36}$$

Equation 36 is the linear form of Eq. 35. $Rln\left(\frac{\mu V_M}{hN_A}\right)$ is plotted against $\frac{1}{T}$ to find enthalpy and entropy. ΔH is the slope, while ΔS is the intercept of the plot. From these values, ΔG can be estimated. It is given by Eq. 37.

$$\Delta G = \Delta H - T\Delta S \tag{37}$$

Table 4 represents the enthalpy and entropy of aqueous AEPZ at different concentrations. The table shows that as the concentration of AEPZ increased, the enthalpy also increased, but the entropy decreased. All the values of enthalpy are positive, indicating that the interactions within the molecules are strong. Table 5 represents the Gibbs free energy of aqueous AEPZ at different temperatures and concentrations. At lower concentrations of AEPZ, the values of Gibbs free energy are negative. This implies that entropy contributes more to the change in Gibbs free energy at lower concentrations. While for 0.4 w AEPZ, the values of Gibbs free energy are positive. At this concentration, enthalpy has more contribution than entropy. For 0.3 w AEPZ, the values of Gibbs free energy at lower temperatures are positive, while those of Gibbs free energy are negative at higher temperatures. The contribution of entropy increases with an increase in temperature. These data are important for the molecular modeling of CO_2-AEPZ + H_2O interaction.

Table 3 Viscosities of aqueous AEPZ

Viscosity, mPa s				
T/K	wt fraction AEPZ			
	0.1 w	0.2 w	0.3 w	0.4 w
298	1.44478	2.68951	5.76939	14.66618
303	1.2547	2.29007	4.61772	10.86967
308	1.12495	1.99773	3.88507	9.03407
313	0.98051	1.7214	3.23997	7.28213
318	0.88877	1.49877	2.76574	5.81478
323	0.81962	1.31446	2.39269	4.61785
328	0.71352	1.16097	1.99895	3.70969
333	0.65974	1.05293	1.75843	3.11107
338	0.61353	0.95287	1.56443	2.68263
343	0.56759	0.87543	1.38652	2.31671
348	0.52174	0.79842	1.23963	2.02026

The standard uncertainties (u) associated with the measured quantity are u (T) = 0.1 K, $u(y)$ = 0.001, $u(\mu)$ = 0.202 mPa s, solvent = water

Table 4 Enthalpy and entropy of aqueous AEPZ

Weight fraction of AEPZs	ΔH (J/mol)	ΔS (J/mol)
0.1	17,067.03465	96.06221
0.2	20,608.72912	91.93642
0.3	25,890.82244	82.34042
0.4	33,817.546	65.05341

Henery's constant and diffusivity

Table 6 shows the diffusivity of CO_2 in AEPZ + H_2O at various concentrations. It is observed from Table 6 that the diffusivity decreased with increasing concentrations of AEPZ in H_2O. It implies that higher the viscosity, the lower the diffusivity. Lower diffusivity may lower the absorption of CO_2 in the viscous solvents (Fang et al. 2020). Again, diffusivity increased with increasing the temperatures.

Table 7 represents Henry's constants of N_2O and CO_2 at different concentrations of aqueous AEPZ at 313 K. It can be observed from Table 7 that Henry's constant increased with an increase in concentrations. Table 8 represents Henry's constant of 0.3 w AEPZ at different temperatures. The physicochemical properties like density, viscosity, diffusivity,

Table 5 Gibbs free energy of aqueous AEPZ

Gibbs free energy (J/mol)				
T, K	wt fraction of AEPZ			
	0.1 w	0.2 w	0.3 w	0.4 w
298	− 11,573.91	− 6802.11	1341.02	14,421.87
303	− 12,054.22	− 7261.80	929.32	14,096.60
308	− 12,534.53	− 7721.48	517.62	13,771.34
313	− 13,014.84	− 8181.16	105.92	13,446.07
318	− 13,495.16	− 8640.84	− 305.78	13,120.80
323	− 13,975.47	− 9100.52	− 717.48	12,795.54
328	− 14,455.78	− 95,60.21	− 1129.19	12,470.27
333	− 14,936.09	− 10,019.89	− 1540.89	12,145.00
338	− 15,416.40	− 10,479.57	− 1952.59	11,819.74
343	− 15,896.71	− 10,939.25	− 2364.29	11,494.47
348	− 16,377.02	− 11,398.94	− 2775.99	11,169.20

Table 6 Diffusivities of aqueous AEPZ

Diffusivity, $\times 10^9$ (m^2/s)				
T (K)	wt fraction AEPZ			
	0.1 w	0.2 w	0.3 w	0.4 w
298	1.39205	0.84676	0.438415	0.217994
303	1.57429	0.97283	0.525249	0.279862
308	1.78447	1.12716	0.629486	0.33706
313	2.04555	1.30397	0.752333	0.411307
318	2.2865	1.50527	0.885171	0.508833
323	2.52024	1.72716	1.03555	0.63209
328	2.8807	1.95149	1.22649	0.770467
333	3.21947	2.21494	1.42565	0.931009
338	3.51538	2.47181	1.62509	1.07992
343	3.93048	2.77904	1.87518	1.27578
348	4.37334	3.11165	2.49375	1.48064

Table 7 Henry's constant of N_2O and CO_2 in aqueous AEPZ at 313 K

(wt. fraction of AEPZ)	Henry's constant of N_2O in AEPZ + H_2O (kPa-l/mol)	Henry's constant of CO_2 in AEPZ + H_2O (kPa-l/mol)
0.1	6395.84	4585.648367
0.2	6880.509	4926.328298
0.3	7336.042	5259.74837
0.4	7756.482	5561.192746

Table 8 Henry's constant of N_2O and CO_2 in aqueous AEPZ for 0.3 w AEPZ

Temperature (K)	Henry's constant of N_2O in AEPZ + H_2O (kPa-l/mol)	Henry's constant of CO_2 in AEPZ + H_2O (kPa-l/mol)
303.15	5887.172	4297.214996
313.15	7336.042	5259.74837
323.15	9056.412	6385.037722
333.15	11,263.904	7941.384727

and Henry's constant are essential for analyzing absorption kinetics and are used in this work. The absorption kinetics of CO_2 in amine solvents depends on these properties. Density and viscosity help determine the liquid-film thickness, while diffusivity and Henry's constant are used in calculating the rate of absorption of CO_2 into amine solvent (Paul et al. 2009a, b) (Table 8).

Determination of k_L and k_2

Table 9 shows the experimental kinetic data for the AEPZ + H_2O system at 313 K including the values of k_L and k_2. Table 10 shows the experimental kinetic data for the AEPZ + H_2O system with AEPZ concentration of 0.3 w. Tables 9 and 10 show that the reaction rate constant has increased with the increase in temperature and concentration. The rate of absorption has also increased. The values of *Ha* are greater than 3 and lesser than E_i in all the cases, proving the pseudo-first-order system's validity. The condition given in Eq. 29 is fulfilled. Temperature dependency of the second-order rate constant mass transfer coefficient has been determined using the Arrhenius equation. The regression of temperature vs. k_2 data is conducted to determine the Arrhenius constant and activation energy. Arrhenius equation is represented in Eq. 38.

$$k_2 = k_0 exp\left(\frac{-E_A}{RT}\right) \tag{38}$$

where k_0 is Arrhenius constant, E_A is the activation energy, and R is the gas constant. After regression of data using Origin software (V-2021) for 30 wt% AEPZ, the following Arrhenius equation is obtained and presented in Eq. 39.

$$k_2 = 6.126 \times 10^{11} exp\left(\frac{-5101.98}{T}\right) \tag{39}$$

The activation energy for the reaction is 42.42 kJ/mol. The activation energy is very high, which indicates that the reaction between aqueous AEPZ and CO_2 is fast. Figure 8 shows the Arrhenius plot for 0.3 w AEPZ at different temperatures. The results obtained in this work are compared with those reported by Paul et al. (2009b) and presented in Fig. 9. It is evident from Fig. 9 that at a low temperature of around 303 K, the values are in good agreement with those reported by Paul et al. (2009b), but at the higher temperature of 353 K, the values are lower than that obtained by them. This minor

Table 9 Kinetic parameter for aq. AEPZ solutions at 313 K

Conc (wt fraction)	K_{ov} (mol/m^2s-kPa)	k_{obs} (/s)	k_2 (L/mol-s)	$N_{CO2} \times 10^2$ (mol/m^2s)	$k_L \times 10^5$ (m/s)	Ha = E	E_i
0.1	0.000252	682.327	887.175	0.192	1.36	85.136	140.410
0.2	0.00168	54,903.218	37,712.86	1.28	7.32	117	313.808
0.3	0.00186	127,239.66	53,712.55	1.634	8.59	121.632	426.544
0.4	0.00208	325,309.3	102,234.2	1.69	10.5	110	656.288

Table 10 Kinetic parameters for 0.3 w AEPZ solutions

Temp (K)	K_{ov} (mol/m^{2}s-kPa)	k_{obs} (/s)	k_2 (L/mol-s)	$N_{CO2}\times10^2$ (mol/m^{2}s)	$k_L\times10^5$ (m/s)	Ha = E	E_i
303.15	0.00141	69,086.56	29,004.39	1.178	2.63	230	368.46
313.15	0.00186	127,239.66	53,712.55	1.282	8.59	121.63	426.54
323.15	0.00222	195,930.04	83,204.58	2.879	11.3	125	348.80
333.15	0.00263	315,841.9	134,996.60	2.957	35.5	28.6	496.66

discrepancy may be due to unpredictable physical properties like solubility and diffusivity; uncertainty in the determination of exact gas–liquid contact area; possible turbulence at the interface, as highlighted by Aboudheir et al. (2003). The experimental results show that AEPZ has excellent potential to be used as a promoter. It can be blended with conventional amines. It has a high CO_2 absorption rate. The values of k_2 for aqueous AEPZ solutions obtained in this work are compared with the results of aqueous MEA reported by Ying and Eimer (2013) at similar concentrations. The comparison is presented in Fig. 10. It is evident from Fig. 10 that AEPZ has a higher rate than MEA and hence is suitable for rate promoter in a solvent blend for CO_2 capture. However, more studies need to be done on oxidative degradation, foaming potential, and environmental impacts for making AEPZ suitable for replacing conventional solvents.

One of the environmental impacts comes if the flue gas contains NOx. Nitrogen dioxide (NO_2) can react with aqueous AEPZ in the absorber of the amine scrubbing system and may form n-nitrosoAEPZ, like other amines reported by Fine et al. (2013) and Du et al. (2013). Although nitrosamines are ubiquitous in our environment, many nitroso compounds are carcinogenic in animals and humans. Hence their emission into the atmosphere is a concern. Fortunately, the trace amount of n-nitrosoAEPZ produced in the absorber can decompose thermally at the regenerator of the scrubbing system as it operates at a higher temperature of about 120 °C, releasing the absorbed NO_2, hence maintaining the balance. These all happen if the amine scrubber treats flue gas without NOx removal. Du et al. (2013) reported that a 5 m PZ/2 m AEPZ blended solvent has a milder nitrosamine formation than piperazine-based solvents. Hence, the addition of AEPZ has decreased nitrosamine formation. This indicates that AEPZ is less prone to forming environmentally hazardous nitrosamine. Again,

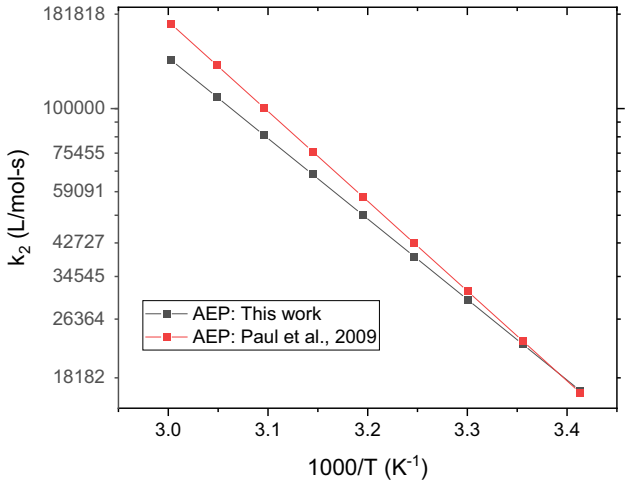

Fig. 9 Comparison of the k_2 with literature-reported data

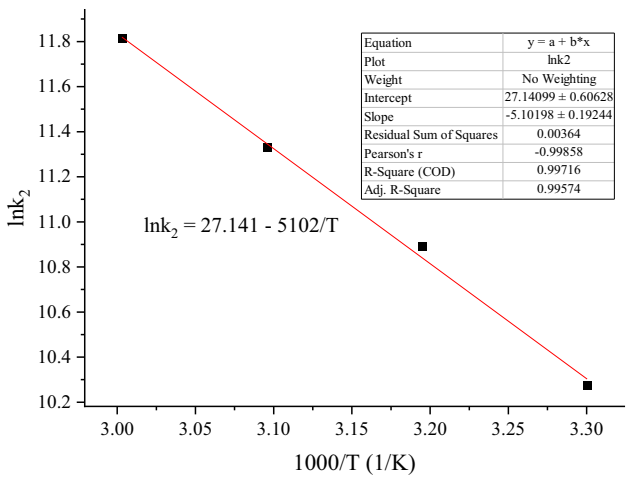

Fig. 8 Arrhenius plot for 0.3 w AEPZ at different temperatures: ■, lnk2; —, Linear fit.$_2$

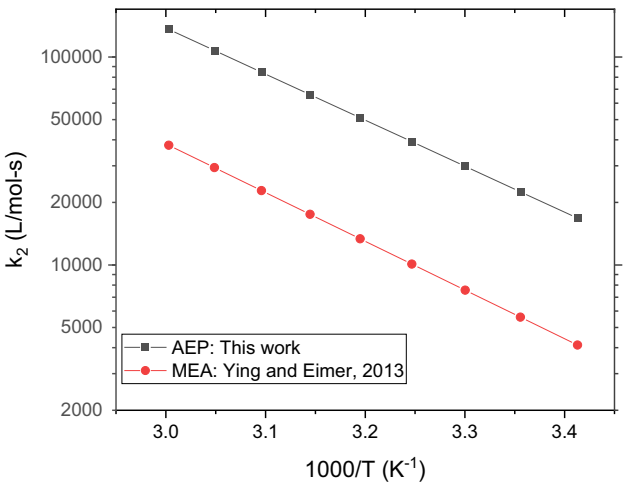

Fig. 10 Comparison of the 2nd-order rate constant, k_2 of AEPZ with MEA

AEPZ has the advantage of higher solubility, lower solvent loss to the environment, and lower nitrosamine formation rate, making this solvent a softer environmental concern.

Conclusion

This work uses a stirred cell reactor to investigate the essential physicochemical properties and CO_2 absorption kinetics of aqueous AEPZ solutions. The studies on density, viscosity, and diffusivity of various weight fractions of aqueous AEPZ are presented at temperatures ranging from 298.15 to 348.15 K at atmospheric pressure. The models based on Redlich–Kister equations are developed from the experimental data, and it is found that the model-predicted data and the experimental data are very close to each other. Henry's constant of N_2O in aqueous AEPZ and kinetic studies of CO_2 in aqueous AEPZ are performed using stirred cell reactor. Both kinetics of CO_2 absorption and solubility of N_2O studies in AEPZ are performed at the concentration ranges of 0.1 to 0.4 weight fraction of AEPZ + H_2O, and at a temperature of 313 K. The same studies are performed for 0.3 weight fraction AEPZ at temperatures raining from 303 to 333 K. Using the experimental results, kinetic parameters are calculated. It is found that the experimental results agree with the assumption of pseudo-first-order kinetics. The second-order rate coefficients of 0.3 w AEPZ at different temperatures are modeled using the Arrhenius equation, with obtained results of the activation energy of 42.42 kJ/mol and the Arrhenius constant of 6.126×10^{11} for 0.3 w AEPZ. The values of aqueous AEPZ have been found to be higher than the values of aqueous MEA, as AEPZ has better absorption kinetics than MEA. Besides, AEPZ has less nitrosamine emission and a lower environmental impact than other solvents. All these properties favor the solvent to be used in the CO_2 capture process and can make the process cost-effective.

Abbreviations

AEPZ: 1-(2-Aminoethyl)piperazine;
DEA: Diethanolamine; *DGA*: Diglycolamine;
DIPA: Diisopropanolamine;
MDEA: Methyldiethanolamine;
MEA: Monoethanolamine; *PZ*: Piperazine

Notation

A: Interfacial area (m^2); Ai: Pair parameters; *[AEPZ]*: Concentration of AEPZ (mol/L); *a, b, c*: Parameters; C_A: Concentration of gas; C_l: Concentration of liquid; C_{N_2O}: Concentration of N2O (mol/L); CO_2: Carbon dioxide; D_{CO_2-AEPZ}: Diffusivity of CO_2 in AEPZ (m^2/s); $D_{CO_2-H_2O}$: Diffusivity of CO_2 in H_2O (m^2/s); $D_{N_2O-AEPZ}$: Diffusivity of N_2O in AEPZ (m^2/s); $D_{N_2O-H_2O}$: Diffusivity of N_2O in H_2O (m^2/s); E: Enhancement factor; E_A: Activation energy; E_i: Instantaneous enhancement factor; H_2O: Water; H_{CO_2-AEPZ}: Henry's constant of CO_2 in AEPZ (kmol/m^3-kPa); $H_{CO_2-H_2O}$: Henry's constant of CO_2 in H_2O (kmol/m^3-kPa); $H_{N_2O-AEPZ}$: Henry's constant of N_2O in AEPZ (kmol/m^3-kPa); $H_{N_2O-H_2O}$: Henry's constant of N_2O in H_2O (kmol/m^3-kPa); *Ha*: Hatta number; ΔH: Enthalpy; h: Planck's constant; ΔG: Gibbs free energy; J_{CO_2}: Absorption flux of CO_2 (mol/m^2 s); k_0: Arrhenius constant; k_2: Second-order reaction rate constant (L/mol-s) or (m^3/kmol-s); k_G: Gas-phase mass transfer coefficient; k_L: Liquid-phase mass transfer coefficient (m/s); $k_{m,}n$: Reaction constant of (m, n)th order; K_{ov}: Overall reaction rate constant (mol/m^2 s–kPa); k_{obs}: Observed kinetic constant (s^{-1}); *kPa*: Kilopascal; M_A: Molecular weight of AEPZ.; M_w: Molecular weight of water; m: Dimensionless solubility; *mPas*: Millipascal-seconds; N_A: Avogadro's number; n: Number of moles; n_1: Number of moles at initial reading; n_2: Number of moles at next reading; n_{CO_2}: Moles of CO_2; N_{CO_2}: Specific rate of absorption of AEPZ (mol/m^2 s); N_2O: Nitrous oxide; P: Pressure of the gas (kPa); $P_{initial}$: Initial pressure (kPa); P_{final}: Pressure at the end of the experiment (kPa); P_t: Pressure at a particular time (kPa); P_{total}: Total pressure (kPa); Pv: Vapor pressure (kPa); P_{CO2}: Partial pressure of CO_2 (kPa); P_{N_2O}: Partial pressure of N_2O (kPa); *ppm*: Parts per million; r: Rate of reaction; R: Gas constant (kPa m^3/mol K); ΔS: Entropy; t: Time (s); t_w: Flow time for the water (s); t_s: Flow time for the solution (s); T: Temperature (K); V: Molar volume of the gas (m^3); V_M: Molar volume (liquid) (m^3); V_G: Volume of the gas (m^3); V_L: Volume of the liquid (m^3); w: Mass fraction; x_A: Mole fraction of AEPZ.; x_w: Mole fraction of water; z: Stoichiometric coefficient; ρ_A: Density of AEPZ (kg/m^3); ρ_m: Density of mixtures (kg/m^3); ρ_s: Density of the solution (kg/m^3); ρ_w: Density of water (kg/m^3); ϑA: Kinematic viscosity of AEPZ (cSt); ϑw: Kinematic viscosity of water (cSt); ϑm: Kinematic viscosity of mixture (cSt); μ: Dynamic viscosity (cP); μ_s: Dynamic viscosity of the solution (cP); μ_w: Dynamic viscosity of water (cP)

Supplementary Information The online version contains supplementary material available at https://doi.org/10.1007/s11356-023-28443-7.

Author contribution Sukanta Kumar Dash: project administration, supervision, conceptualization; resources; analysis and interpretation, methodology; review and editing. Ishanee Sharma: experimentation; writing—original draft; validation; writing—review and editing. All authors read and approved the final manuscript.

Funding Financial support is provided by the Department of Biotechnology (DBT) through the project "Integrated Design and Demonstration of Intensified CO2 Capture with cost-effective advanced Process. (INDIA-CO2)," No. T/PR31120/PBD/26/755/2019.

Data availability All data generated or analyzed during this study are included in this published article (and its supplementary information files).

Declarations

Ethical approval and concent to participate Not applicable.

Consent for publication Not applicable.

Competing interests The authors declare no competing interests.

References

Aboudheir A, Tontiwachwuthikul P, Chakma A, Idem R (2003) Kinetics of the reactive absorption of carbon dioxide in high CO_2-loaded, concentrated aqueous monoethanolamine solutions. Chem Eng Sci 58:5195–5210. https://doi.org/10.1016/j.ces.2003.08.014

Águila-Hernández J, Trejo A, García-Flores BE, Molnar R (2008) Viscometric and volumetric behaviour of binary mixtures of sulfolane and N-methylpyrrolidone with monoethanolamine and diethanolamine in the range 303–373K. Fluid Phase Equilib 267:172–180. https://doi.org/10.1016/j.fluid.2008.02.023

Bhosale RR, Mahajani VV (2013) Kinetics of absorption of carbon dioxide in aqueous solution of ethylaminoethanol modified with N-methyl-2-pyrolidone. Sep Sci Technol 48(15):2324–2337. https://doi.org/10.1080/01496395.2013.805228

Choi JH, Kim YE, Nam SC, Yun SH, Yoon YI, Lee J-H (2016) CO_2 absorption characteristics of a piperazine derivative with primary, secondary, and tertiary amino groups. Korean J Chem Eng 33:3222–3230. https://doi.org/10.1007/s11814-016-0180-9

Coulson JM, Richardson JF, Backhurst JR, Harker JH (1999) Fluid flow, heat transfer and mass transfer. Butterworth-Heinemann

Danckwerts PV, Kennedy AM, Roberts D (1963) Kinetics of CO_2 absorption in alkaline solutions—II: Absorption in a packed column and tests of surface-renewal models. Chem Eng Sci 18(2):63–72. https://doi.org/10.1016/0009-2509(63)80015-9

Das B, Deogam B, Mandal B (2017) Experimental and theoretical studies on efficient carbon dioxide capture using novel bis(3-aminopropyl)amine (APA)-activated aqueous 2-amino-2-methyl-1-propanol (AMP) solutions. RSC Adv 7:21518–21530. https://doi.org/10.1039/C7RA01286A

Dash SK, Bandyopadhyay SS (2016) Studies on the effect of addition of piperazine and sulfolane into aqueous solution of N-methyldiethanolamine for CO2 capture and VLE modelling using eNRTL Eq. Int J Greenhouse Gas Control 44:227–237. https://doi.org/10.1016/j.ijggc.2015.11.007

Dash SK, Wadibhasme L (2017) Retrofitting a CO2 capture unit with a coal based power plant: process simulation and parametric study. J Clean Energy Tech 5:248–253. https://doi.org/10.18178/JOCET.2017.5.3.377

Dash SK, Samanta AN, Bandyopadhyay SS (2011) Solubility of carbon dioxide in aqueous solution of 2-amino-2-methyl-1-propanol and piperazine. Fluid Phase Equilib 307(2):166–174. https://doi.org/10.1016/j.fluid.2011.05.009

Dash SK, Samanta AN, Bandyopadhyay SS (2012) Experimental and theoretical investigation of solubility of carbon dioxide in concentrated aqueous solution of 2-amino-2-methyl-1-propanol and piperazine. J Chem Thermodyn 51:120–125. https://doi.org/10.1016/j.jct.2012.02.012

Dash SK, Samanta AN, Bandyopadhyay SS (2014) Simulation and parametric study of post combustion CO2 capture process using (AMP+PZ) blended solvent. Int J Greenhouse Gas Control 21:130–139. https://doi.org/10.1016/j.ijggc.2013.12.003

Dey A, Dash SK, Mandal B (2018) Equilibrium CO2 solubility and thermophysical properties of aqueous blends of 1-(2-aminoethyl) piperazine and N-methyldiethanolamine. Fluid Phase Equilib 463:91–105. https://doi.org/10.1016/j.fluid.2018.01.030

Dey A, Dash SK, Balchandani SC, Mandal B (2019) Investigation on the inclusion of 1-(2-aminoethyl) piperazine as a promoter on the equilibrium CO_2 solubility of aqueous 2-amino-2-methyl-1-propanol. J Mol Liq 289. https://doi.org/10.1016/j.molliq.2019.111036

Du Y, Li L, Namjoshi O, Voice AK, Fine NA, Rochelle GT (2013) Aqueous piperazine/N-(2-aminoethyl) piperazine for CO_2 capture. In: Energy Procedia. Elsevier Ltd, 1621–1638. https://doi.org/10.1016/j.egypro.2013.06.038

Fang C, Du X, Wang L, Fu D (2020) Investigation of viscosity for AEPZ aqueous solutions. In: IOP Conference Series: Earth and Environmental Science. IOP Publishing Ltd. https://doi.org/10.1088/1755-1315/514/5/052019

Fine NA, Goldman MJ et al (2013) Managing n-nitrosopiperazine and dinitrosopiperazine. Energy Procedia 37:273–284

IPCC (2021) https://www.ipcc.ch/report/ar6/wg1/downloads/report/IPCC_AR6_WGI_SPM.pdf (Accessed 20 September 2021)

Kierzkowska-Pawlak H, Chacuk A, Siemieniec M (2014) Reaction kinetics of CO_2 in aqueous 2-(2-aminoethylamino)ethanol solutions using a stirred cell reactor. Int J Greenhouse Gas Control 24:106–114. https://doi.org/10.1016/j.ijggc.2014.03.004

Li L, Zhang J, Li Q, Guo B, Zhao T, Sha F (2014) Density, viscosity, surface tension, and spectroscopic properties for binary system of 1,2-ethanediamine + diethylene glycol. Thermochim Acta 590:91–99. https://doi.org/10.1016/j.tca.2014.05.034

Lu C, Chen M, Luo X, Liang Z (2019) The effects of mass transfer on the determination of gas-liquid reaction kinetics in a stirred cell reactor: in the case of CO_2 absorption by aqueous alkanolamine solution. Energy Fuels. https://doi.org/10.1021/acs.energyfuels.9b02986

Monteiro JGMS, Knuutila H, Penders-van Elk NJMC, Versteeg G, Svendsen HF (2015) Kinetics of CO_2 absorption by aqueous N, N-diethylethanolamine solutions: literature review, experimental results and modelling. Chem Eng Sci 127:1–12. https://doi.org/10.1016/j.ces.2014.12.061

NOAA (2021) https://gml.noaa.gov/ccgg/trends/data.html (accessed 20 September 2021)

Park MK, Sandall OC (2001) Solubility of carbon dioxide and nitrous oxide in 50 mass methyldiethanolamine. J Chem Eng Data 46(1):166–168. https://doi.org/10.1021/je000190t

Paul S, Ghoshal AK, Mandal B (2009a) Kinetics of absorption of carbon dioxide into aqueous blends of 2-(1-piperazinyl)-ethylamine and N-methyldiethanolamine. Chem Eng Sci 64:1618–1622. https://doi.org/10.1016/j.ces.2008.12.034

Paul S, Ghoshal AK, Mandal B (2009b) Kinetics of absorption of carbon dioxide into aqueous solution of 2-(1-piperazinyl)-ethylamine. Chem Eng Sci 64:313–321. https://doi.org/10.1016/j.ces.2008.10.025

Tiseo I (2022) https://www.statista.com/statistics/1129656/global-share-of-co2-emissions-from-fossil-fuel-and-cement/ (Accessed 21 April 2022)

Vaidya PD, Kenig EY (2007) CO2-alkanolamine reaction kinetics: a review of recent studies. Chem Eng Technol 30(11):1467–1474

Versteeg GF, van Swaaij WPM (1988) Solubility and diffusivity of acid gases (carbon dioxide, nitrous oxide) in aqueous alkanolamine solutions. J Chem Eng Data 33:29–34. https://doi.org/10.1021/je00051a011

Vogel H, Weiss A (1982) Transport properties of liquids, III. Viscosity of athermal liquid mixtures. Ber Bunsenges Phys Chem 86:193–198. https://doi.org/10.1002/bbpc.19820860304

Ying J, Eimer DA (2013) Determination and measurements of mass transfer kinetics of CO_2 in concentrated aqueous monoethanolamine solutions by a stirred cell. Ind Eng Chem Res 52:2548–2559. https://doi.org/10.1021/ie303450u